Fullerene-modified polyamide 6 by in situ anionic polymerization in the presence of PCBM

Nadya Dencheva, Hugo Gaspar, Sergej Filonovich, Olga Lavrova, Tito Busani, Gabriel Bernardo & Zlatan Denchev

Journal of Materials Science
Full Set - Includes `Journal of Materials Science Letters'

ISSN 0022-2461
Volume 49
Number 14

J Mater Sci (2014) 49:4751-4764
DOI 10.1007/s10853-014-8174-7

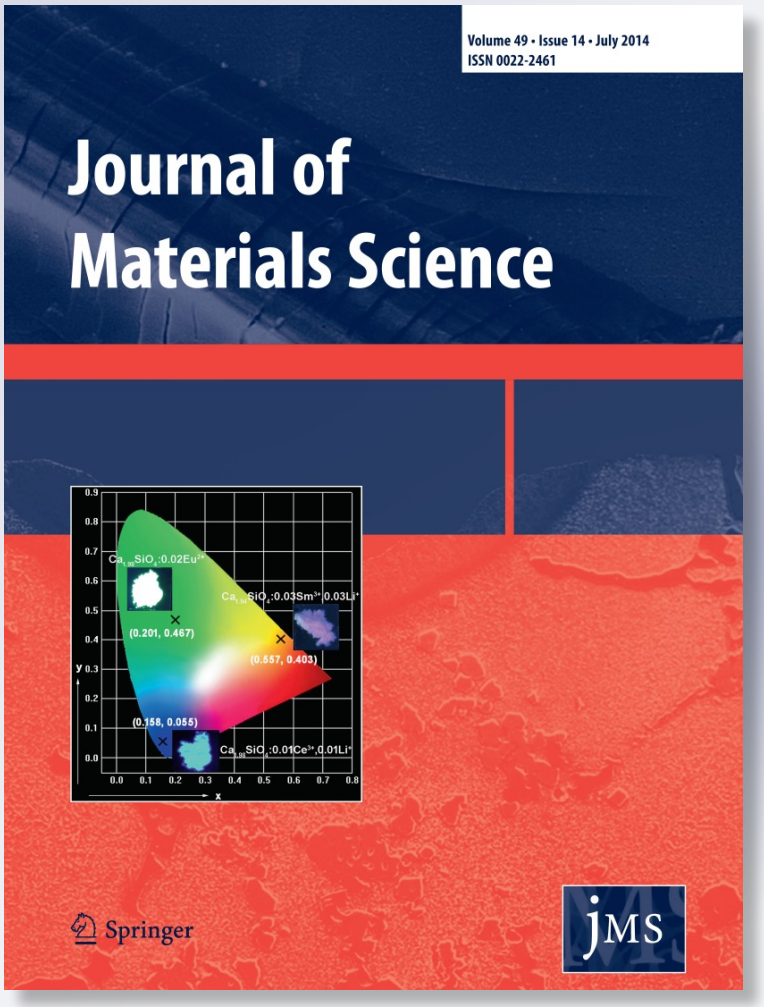

Springer

J Mater Sci (2014) 49:4751–4764
DOI 10.1007/s10853-014-8174-7

Fullerene-modified polyamide 6 by in situ anionic polymerization in the presence of PCBM

Nadya Dencheva · Hugo Gaspar · Sergej Filonovich · Olga Lavrova · Tito Busani · Gabriel Bernardo · Zlatan Denchev

Received: 13 January 2014 / Accepted: 13 March 2014 / Published online: 29 March 2014

Abstract Activated anionic ring-opening polymerization of ε-caprolactam (ECL) was carried out for the first time in the presence of [6,6]-phenyl-C_{61}-butyric acid methyl ester (PCBM) to prepare polyamide 6 (PA6)-based composites comprising up to 3 wt% of this fullerene derivative. This in situ polymerization process produced high molecular weight composites containing 52–80 % of gel fraction at PCBM concentration ≥0.5 wt%. Spectral, thermo-mechanical, synchrotron X-ray, and scanning electron microscopy data were used to elucidate the structure and morphology of the PA6/PCBM composites. A mechanism of the chemical structure evolution was proposed starting with incipient complexation between ECL and PCBM, via subsequent chemical linking of ECL moieties on the C_{60} spheroid and final formation of star-burst and cross-linked morphologies. PCBM amounts of 0.1 wt% and more decreased the volume resistivity from 10^{12} Ω cm (neat PA6) to 10^{9}–10^{7} Ω cm, thus opening the way for new applications of anionic PA6.

N. Dencheva · H. Gaspar · G. Bernardo · Z. Denchev (✉)
Institute for Polymers and Composites/I3N, University of Minho, 4800-058 Guimarães, Portugal
e-mail: denchev@dep.uminho.pt

S. Filonovich
CENIMAT/I3N, New University of Lisbon, 2829-516 Caparica, Portugal

O. Lavrova · T. Busani
Electrical and Computer Engineering, University of New Mexico, Albuquerque, NM 87106, USA

Introduction

Buckminsterfullerene C_{60} and its functionalized derivatives have attracted considerable attention due to their large number of potential applications in organic photovoltaics [1], organic field effect transistors [2], quantum information processing [3], as antioxidants and biopharmaceuticals [4], and in water purification systems [5]. Polymer composites suitable for preparation of electronic and optical materials with appropriate photoinduced electron transfer or photoexcitation properties may be based on conjugated polymer matrices modified by fullerene compounds [6, 7]. Conventional polymers such as polyethylene [8, 9] and polystyrene [10–13] have also been tested as matrices for fullerenes. These studies have shown that pristine C_{60} has low compatibility to polymers resulting in insufficient properties of the final composite. In an attempt to improve the compatibility of C_{60}, efforts have been made to functionalize the fullerene structure by producing monosubstituted derivatives. The use of [6,6]-phenyl-C_{61}-butyric acid methyl ester (PCBM) and [5,6]-phenyl-C61-butyric acid cholesteryl has been reported in conjugated polymer/polystyrene or polyethylene systems obtained by gel processing [11]. Lu et al. [8] studied benzylaminofullerene/polyethylene solution cast systems proving aggregation of the functionalized C_{60} into micron-sized domains.

An alternative way to increase the dispersion of mineral fillers in polymer composites would be to synthesize the matrix in situ, i.e., by initially mixing the filler with the monomer and then polymerizing this system. Because of the low viscosity of the monomer, in situ polymerization techniques can disperse quite effectively particulate or layered fillers in polymer matrices [14]. Activated anionic ring-opening polymerization (AAROP) of lactams

to *n*-polyamides is a good example of such in situ matrix creation process that can be used for the preparation of polyamide/C_{60} fullerene composites. Kelar [15] performed AAROP of ε-caprolactam (ECL) containing of up to 0.3 wt% of a C_{60}/C_{70} mixture proving that fullerenes do not inhibit the polymerization to polyamide 6 (PA6). Thermogravimetric and mechanical investigations showed that the carbon allotrope acted as thermal stabilizer of PA6 and increased the stress at break and the Young's modulus, while elongation at break and impact strength were decreased slightly. Zuev and Ivanova [16] studied the effect of fulleroid fillers (C_{60}, mixture of C_{60}/C_{70} and fulleroid soot) on the mechanical, tribological and electrical properties of nanocomposites based on PA6 prepared by in situ AAROP. Both tensile modulus and strength of the polymer nanocomposites were found to improve with up to 15 % upon the addition of 0.001–0.1 wt% of fulleroid materials. This reinforcement effect was attributed to the selective crystallization of PA6 in its α-form, promoted by the fullerenes. Scratch tests showed that the addition of the fulleroid fillers decreases the friction coefficient of the nanocomposites to approximately half of the value observed on neat PA6. Electrical volume resistivity was found to decrease with the loading of fillers being $\sim 10^7\ \Omega$ cm at 0.1 wt% loading.

The effect of C_{60} on the mechanical and dielectric properties of nanocomposites based on polyamide 12 (PA12), prepared by in situ AAROP, was also studied [17, 18]. A 20 % improvement of the Young's modulus and tensile strength values was observed by the addition of only 0.02–0.08 wt% of C_{60}. Dielectric spectroscopy results showed that the segmental relaxation processes become faster with the addition of C_{60}. This effect was associated with the decrease of the glass transition temperature. At the same time, the secondary or γ relaxation process of PA12/C_{60} nanocomposites slowed down.

All of the PA6-based composites prepared so far by AAROP have been obtained only with pristine fullerenes. To the best of our knowledge, no attempts have been made to carry out the AAROP in the presence of functionalized C_{60} that are easily soluble in the monomer. The combination of more organophylic fullerene derivative with in situ preparation of the PA6 matrix could positively influence the dispersion of the filler and, therefore, the composite properties. The aim of this study is to prepare PA6/PCBM composites by AAROP, to assess the effect of PCBM constituent on the structure, morphology, thermal, and electric properties of the composites and, on this basis, to elucidate the mechanism of PCBM incorporation.

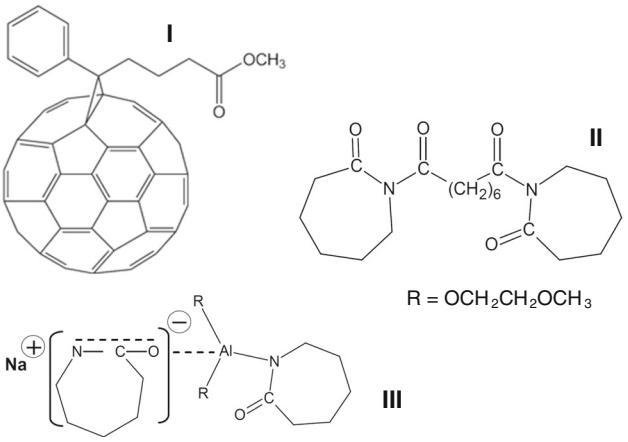

Scheme 1 Chemical structures of *I* PCBM, *II* C20 (activator), and *III* DL (initiator)

Experimental

Materials

Carbon nanoparticles of PCBM (Scheme 1, I) with greater than 99 % purity were acquired from Solenne BV. The ECL monomer with reduced moisture content suitable for AAROP (AP-Nylon® caprolactam) was delivered from Brüggemann Chemical, Germany. Before use, it was kept under vacuum for 1 h at 23 °C. As polymerization activator, Bruggolen C20P® from Brüggemann Chemical, Germany (C20) was used. According to the manufacturer, it contains 80 wt% of blocked di-isocyanate in ECL. The supposed chemical structure of C20 is presented in Scheme 1, II. The initiator sodium dicaprolactamato-bis-(2-methoxyethoxo)-aluminate (Dilactamate, DL, Scheme 1, III) was purchased from Katchem and used in the form of 80 wt% solution in toluene.

Sample preparation by AAROP

About 0.25 mol of ECL (m.p. 69 °C) were molten in a 250 mL flask at 110 °C under nitrogen flux, and then the desired amounts of PCBM were added at once. The mixture was energetically stirred at the same temperature until complete dissolution of the functionalized fullerene which took up to 5 min. Then, the catalytic system comprising DL and C20 was added. Upon homogenization, the reactive mixture was rapidly transferred into glass test tubes with diameters of ca. 8 mm. They were placed into an oven heated at 170 °C. After 30 min, the temperature was gradually decreased to 30 °C. All samples thus prepared are shaped as cylindrical bars. The degree of monomer conversion

determined by Soxhlet extraction to constant weight with methanol was in the 97–99 % range. Only extracted samples were subjected to further characterization.

Characterization techniques

The average viscosimetric molecular weight M_v was determined by intrinsic viscosity measurements in 97 % sulfuric acid at a concentration of 0.2 g/dL with a suspended level Ubbelohde viscometer thermostated at 23 °C using the Mark–Houwink equation with $K = 10^{-3}$ and $\alpha = 0.7$ [19].

Differential thermal analysis was made in a 200 F3 calorimeter of Netzsch at a heating rate of 10 °C/min under N_2 purge from −20 to 300 °C. Two heating and cooling scans cycles were run with each sample, the sample weights being in the 5–10 mg range. Thermogravimetric measurements were carried out using a TA Q500 thermobalance. The instrument was calibrated with indium and aluminum standards. Samples of ~20 mg were placed in platinum crucibles and heated from 30 to 600 °C using a heating ramp of 10 °C/min under air flow of 50 mL/min.

Dynamic mechanical thermal analysis (DMTA) measurements were performed in tension mode on rectangular shaped bars. The sample free length was 10 mm on which oscillating strain of 20 μm and a constant strain frequency of 1 Hz were applied. The sample was heated at 2 °C/min, from −100 to 180 °C, with the sample oven being continuously purged with nitrogen gas.

Diffuse reflectance infrared Fourier-transform spectroscopy (DRIFTS) was performed in a Perkin–Elmer Spectrum 100 apparatus using the respective attachment at a resolution of 2 cm^{-1} accumulating 16 spectra for better signal-to-noise ratio.

For scanning electron microscopy (SEM) characterization, the samples were cryofractured, and the sections produced were coated with 8-nm-thick Au–Pd alloy (80–20 wt%) using a high-resolution sputter coater (208HR Cressington Company), coupled to a high-resolution thickness controller (MTM-20 Cressington). Morphological analysis of the fractured sections was performed in an ultra-high resolution field emission gun scanning electron microscope NOVA 200 Nano (FEI Company). Secondary electron images were obtained with an acceleration voltage of 5 kV.

For the volume resistivity measurements, disks with a thickness of 2 mm were cut from the initial PA6 bars, cleaned with isopropanol, and blown with dry nitrogen. Aluminum electrical contacts were deposited on them using a thermal evaporator operating at ~10^{-6} torr. Deposition rate was kept at ca. 0.3 nm/s so as to ensure a good contact between the metal and the sample, and to avoid foliation of the metal. The relation between the amount of PCBM and the resistivity of the samples was determined using a semiconductor characterization system Keythley 4200-SCS with Janis ST-500 cryogenic probe station measuring the current as a function of the applied voltage.

The wide-angle X-ray scattering patterns (WAXS) in this study were registered at the Soft Condensed Matter Beamline (A2) of HASYLAB, Hamburg, Germany using synchrotron radiation with a wavelength fixed to 0.15 nm. The sample-to-detector distance was set at 90 mm, and the diffraction patterns being registered by means of a MAR-CCD two-dimensional detector of Rayonix. The samples were studied in transmission mode with an exposure time of 25 s. A sample holder with incorporated heaters and cooling with compressed air was used allowing for controlled heating–cooling cycles in the 30–300 °C range. An Imago multichannel processor and program controller of JUMO GmbH (Germany) were used to regulate the sample temperature. The difference between the read-out and real temperature was found to be 3–4 °C at the heating rate of 20 °C/min applied in this study. Corrections for background scattering, irradiated volume, and beam intensity were performed for each two-dimensional pattern. For further data processing, a commercial software package was used [20] to apply peak fitting in the linear WAXS patterns obtained after integration between scattering angles 2θ of three and 40°.

Results and discussion

Synthesis of the PA6/PCBM materials

The chemistry of the AAROP of ECL is well known since the early 1970s [21]. As seen from Scheme 1, the activator C20 contains two preformed imide links C(O)–N–C(O), in the presence of which polymerization starts directly with the propagation stage [22]. After some optimization experiments, the AAROP temperature was set at 170 °C, which produced neat PA6 with 97–99 % degree of ECL conversion within polymerization times of 15–20 min. The intrinsic viscosity [η] of the anionic homo-PA6 polymerized under the optimized conditions was 2.9 dL/g corresponding to $M_v = 85{,}000$. More information about the polymerization of ECL at similar conditions can be found elsewhere [14].

In the presence of PCBM, the AAROP of ECL showed some peculiarities. In the stage of ECL/PCBM homogenization at 110 °C, the color of the system changed rapidly from colorless to dark red or chestnut brown, depending on the PCBM concentration. Addition of initiator DL resulted in a dark green color which did not change upon addition of the C20 activator. The final polymerizate was dark brown-to-black.

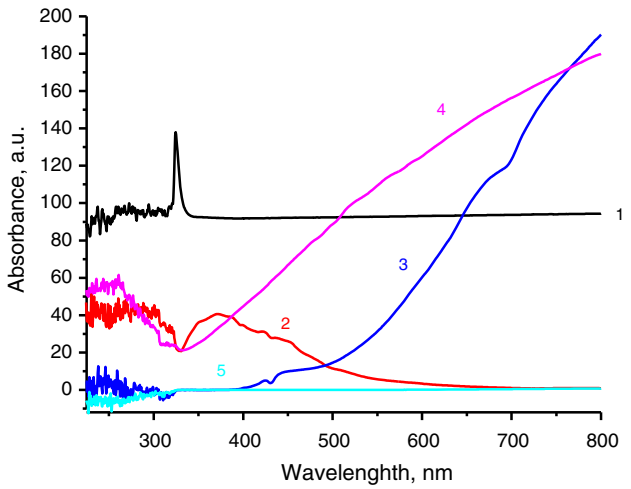

Fig. 1 UV/Vis curves in acetone of ECL, PCBM, and the acetone-soluble fractions of their mixtures with the components of the AAROP catalytic system. *1* ECL, *2* PCBM, *3* ECL+PCBM, *4* ECL+PCBM+DL, *5* ECL+PCBM+DL+C20

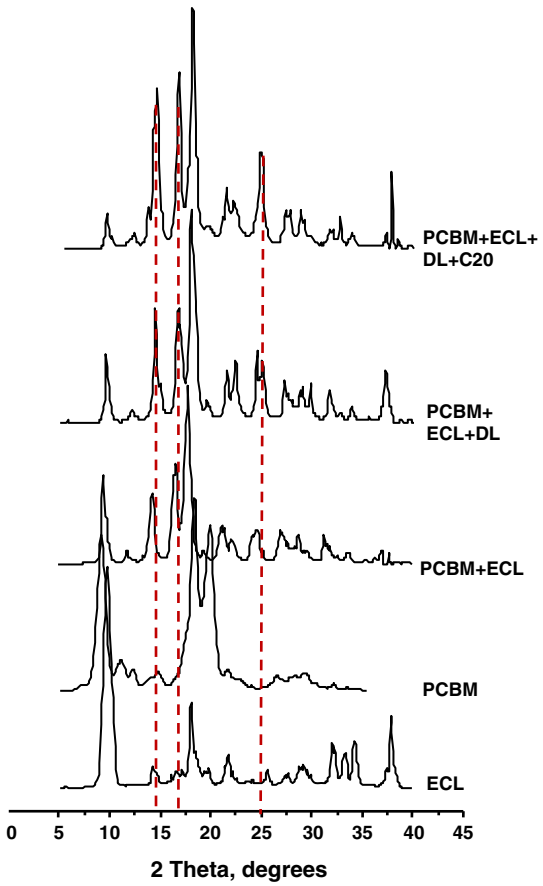

Fig. 2 Synchrotron WAXS patterns of ECL, PCBM, and their mixtures with the polymerization catalytic system components before AAROP. Mixtures obtained at 100 °C, patterns at 30 °C. *Dashed lines* mark the angular position the new crystalline peaks appearing due to ECL–PCBM complexation

The changes of color in the stage of homogenization can be explained with the formation of anion–radical complexes and zwitter ions between the PCBM electron-deficient C_{60} benzene rings and the nucleophilic –NH– groups originating from ECL. The formation of green solutions (fast process) that turn chestnut brown (slow process) was observed previously in solid C_{60} reacting with neat amines [23]. Careful monitoring of these reactions with ESR and UV/Vis spectroscopy showed that the first step is a single-electron transfer from the amine to C_{60} to give the C_{60} radical anion. The next step is a radical recombination and the formation of zwitter ions [24].

In this work, we attempted to study the ECL/PCBM interactions with UV/Vis spectroscopy. Figure 1 shows the absorption curves in acetone of neat ECL, neat PCBM, and the three samples comprising ECL+PCBM, ECL+PCBM+DL, and ECL+PCBM+DL+C20. The latter were obtained by removing aliquot amounts from the AAROP reaction mixture at 110 °C, cooling and dissolving each of them in 10 mL of acetone.

As seen from Fig. 1, the UV/Vis (curve 3) of ECL+PCBM is not a superposition of the ECL and PCBM curves. Curve 3 contains a weaker peak centered at 250 nm characteristic of PCBM, but the other PCBM peak at 360 nm is missing. The narrow peak at 337 nm of the ECL sample most probably due to a H-bond formation with the acetone C=O group is also missing. Instead, a massive band centered above 800 nm appears in curve 3. The addition of the DL anion (curve 4) changes the UV/Vis absorption of the reaction mixture. Apparently, after C20 is added (curve 5), AAROP starts rapidly forming acetone-insoluble PA6. These observations are consistent with the supposition for electron interactions among ECL, PCBM, and DL before AAROP similar to those observed previously in C_{60}/amine mixtures. A possible mechanism of this interaction will be presented further in the text.

More insight into the ECL–PCBM interaction was obtained from the synchrotron WAXS patterns of the AAROP reaction mixture before and after the polymerization. Figure 2 shows clearly that the simple mixing of ECL with PCBM at 110 °C followed by cooling to 30 °C results in three new crystalline reflections centered at 14.4, 16.7, and 24.7° 2θ, while the crystalline peak of neat PCBM at 19.8° almost completely disappears. The three new reflections intensify as the components of the catalytic system DL and C20 are added. This formation of crystalline planes not present in the initial compounds is in agreement with the supposed ECL–PCBM–DL complexation before AAROP.

This complexation process, however, does not disturb the polymerization to proceed at high rate. Within 30 min, the AAROP was completed with 97–99 % conversion to

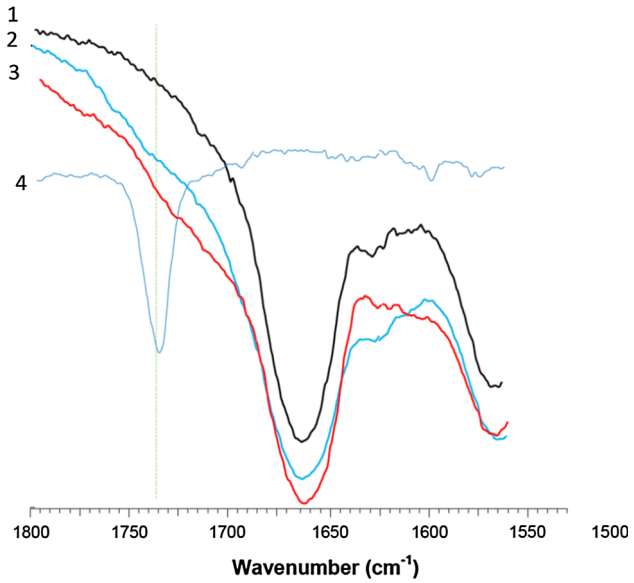

Fig. 3 DRIFTS spectra of *1* neat anionic PA6, *2* PA6 with 1 wt% PCBM, *3* PA6 with 3 wt% PCBM, *4* neat PCBM

high molecular weight of the PA6 matrix. The composites with low percentage of PCBM (0.05 and 0.1 wt%) showed M_v values around 90,000, which is close to that of the neat PA6 with $M_v = 85{,}000$. The M_v for the samples with 0.5–3.0 % PCBM was not determined due to the formation of 52–80 % gel fraction. Apparently, crosslinking of the PA6 chains occurs, involving their random grafting on fullerene spheroids as pointed out by Prato [25].

The supposition of grafting of PA6 chains on fullerene spheroid requires that more fullerene compound will be accumulated in the gel fraction as its concentration in the PA6/PCBM composite grows. Figure 3 gives evidence for such accumulation based on diffuse reflectance FTIR. It shows that neat PA6 (curve 1) shows no peak between 1750 and 1700 cm^{-1}, whereas PCBM (curve 4) has a strong band centered at 1738 cm^{-1} for its ester carbonyl group. The gel fractions of the composites with 1 and 3 % of PCBM (curves 2 and 3) display weak but observable shoulders in this area being slightly better expressed in the latter case. This finding is in good agreement with the random grafting of PA6 on the C_{60} spheroid of PCBM.

X-ray structural studies of the PA6 matrix

Previous studies have shown that the crystalline structure of PA6 is quite sensitive to the presence of inorganic fillers. Figure 4a shows the evolution of the synchrotron WAXS profiles of PA6/PCBM composites comprising up to 1.0 wt% PCBM. The patterns were taken at 30 °C using samples whose AAROP was performed at identical conditions. To enable quantification of the overall degree of crystallinity X_c and the content of the α- and γ-PA6 polymorphs, separation of the crystalline and amorphous scattering of the WAXS curves was performed by peak fitting [26]. Figure 4b shows an example of this deconvolution procedure applied to the composite containing 1 wt% of PCBM. The three shaded peaks are the strongest PCBM crystalline reflections that had to be considered for best fit. The numerical data extracted from the WAXS patterns for all as-prepared PA6/PCBM composites in Fig. 4a are presented in Table 1. Since AAROP is carried out at 170 °C, i.e., below the melting temperature of the forming PA6, it is accompanied by intensive crystallization of polymer chains that have reached a certain critical length. Comparing the WAXS profiles in Fig. 4a and considering their deconvolution in Fig. 4b, it can be concluded that PCBM composites and the neat PA6 matrix contain predominantly the monoclinic α-PA6 polymorph with its two peaks of α(200) and α(002)/(202) crystalline planes. This is the polymorph that formed first in PA6/clay composites prepared by AAROP [14]. The two less intensive reflections in Fig. 4b centered around 22.5° and that at 11.5° 2θ are of the γ-PA6 phase considered to have pseudo-orthorhombic or pseudo-hexagonal lattice. The presence of PCBM does not change significantly X_c which is in the 40–45 % range (Table 1). PCBM loads of ≥0.5 % result in PA6 matrices being almost two times richer in α-PA6 than the neat matrix. This means that the observed complexation at the stage of ECL–PCBM pre-polymerization and the intensive crosslinking during the AAROP have created conditions favoring the formation of the thermodynamically more stable α-PA6 form. The shift of the two α-PA6 reflections toward lower 2θ values in all PCBM composites in Fig. 4a is an indication of expansion of the unit-cell dimensions.

Annealing of the as-prepared composites below the melting point of the PA6 matrix (e.g., between 160 and 200 °C) results in approximation of the two α-reflections, i.e., the presence of PCBM does not impede the α-to-γ form transition characteristic for PA6. Cooling the samples to 30 °C restores the initial WAXS profiles in Fig. 4a. However, if the PA6 matrix is melted at 260 °C and then gradually cooled to 30 °C, the evolution of the crystalline structure built in the presence of PCBM is different (Fig. 5; Table 2).

As seen in Fig. 5, within the 200–170 °C range, the matrix material displays a single crystalline reflection corresponding to γ-PA6. At 150 °C, incipient reflections typical of the α-PA6 phase appear and at 30 °C considerable amounts of both α and γ polymorphs coexist, the former being still predominant. It should be noted that clay-reinforced PA6 composites prepared by AAROP after similar recrystallization showed predominant formation of γ-PA6 crystals [14]. This change in the crystallization behavior agrees with the presence of a network structure in

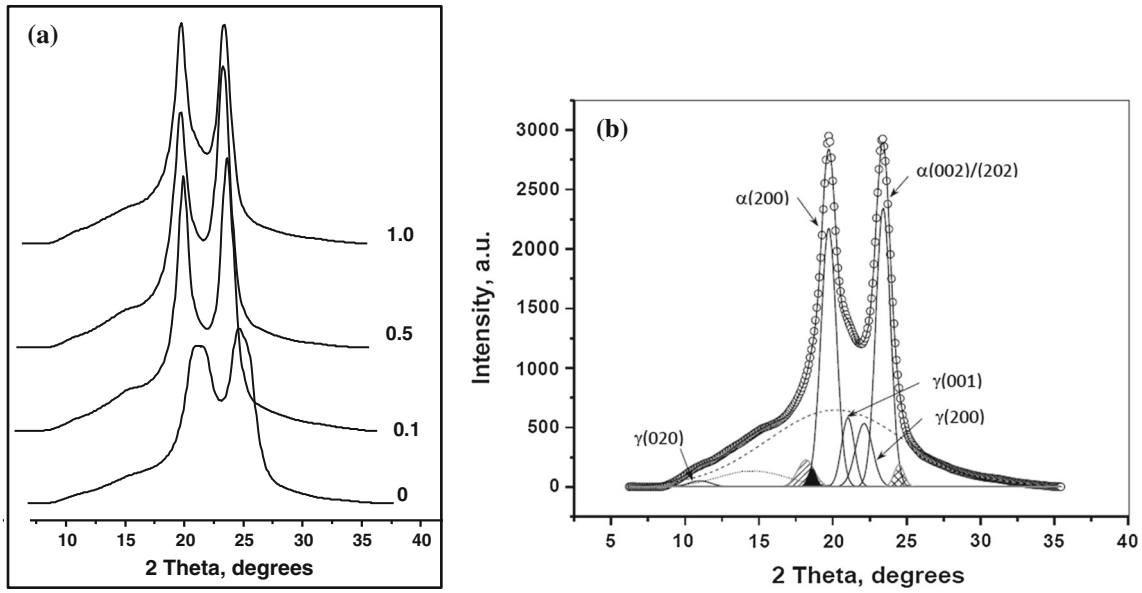

Fig. 4 Evolution of the synchrotron WAXS patterns of PA6 composites: **a** as a function of the amount of PCBM in wt%, **b** example of deconvolution of the sample containing 1 % PCBM, *b*-axis is the chain axis. For more details, see the text. The *shaded peaks* are of PCBM

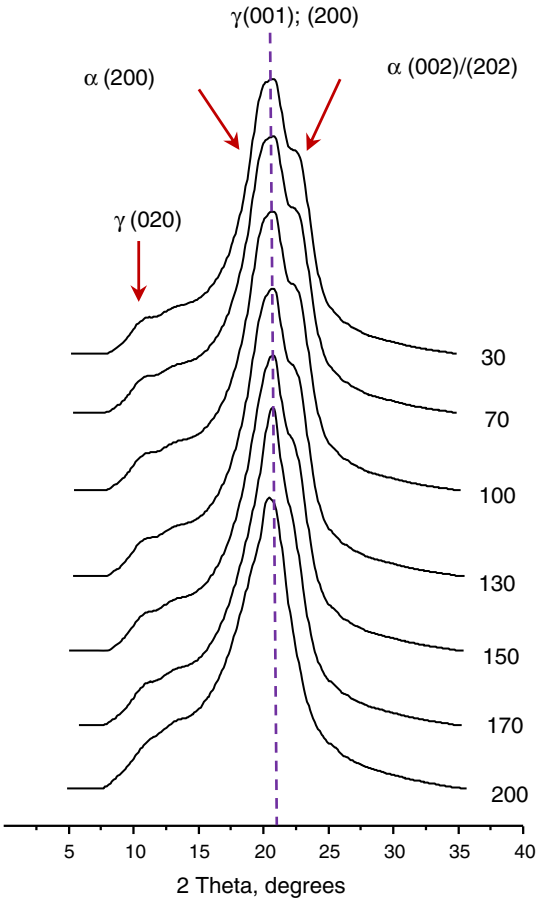

Fig. 5 Dynamic recrystallization of PA6 with 1 wt% of PCBM as revealed by WAXS. The sample is melted at 260 °C and then cooled to 30 °C taking patterns at the indicated temperatures in °C

Table 1 Influence of the PCBM content on the crystalline structure of PA6 matrix in as-prepared composites

PCBM content (wt%)	At 30 °C			
	X_c (%)	α (%)	γ (%)	α/γ
–	41.7	31.3	15.4	2.03
0.1	46.0	32.5	13.5	2.41
0.5	47.1	38.1	9.0	4.23
1.0	46.0	36.7	9.3	3.95

Table 2 Influence of the PCBM content on the crystalline structure of PA6 matrix after melting and recrystallization

PCBM (wt%)	At 30 °C after melting at 260 °C			
	X_c (%)	α (%)	γ (%)	α/γ
–	49.1	33.9	15.2	2.23
0.1	49.7	35.7	14.0	2.55
0.5	50.0	37.0	13.0	2.84
1.0	49.8	36.0	13.8	2.61

the PA6/PCBM systems. Apparently, this network is preserved after matrix melting at 260 °C and upon recrystallization favors such conformations of the PA6 chains that impede the formation of the γ-polymorph.

Thermal properties

The structural investigations made by WAXS correlate with the DSC data. During the first heating scans of the as-

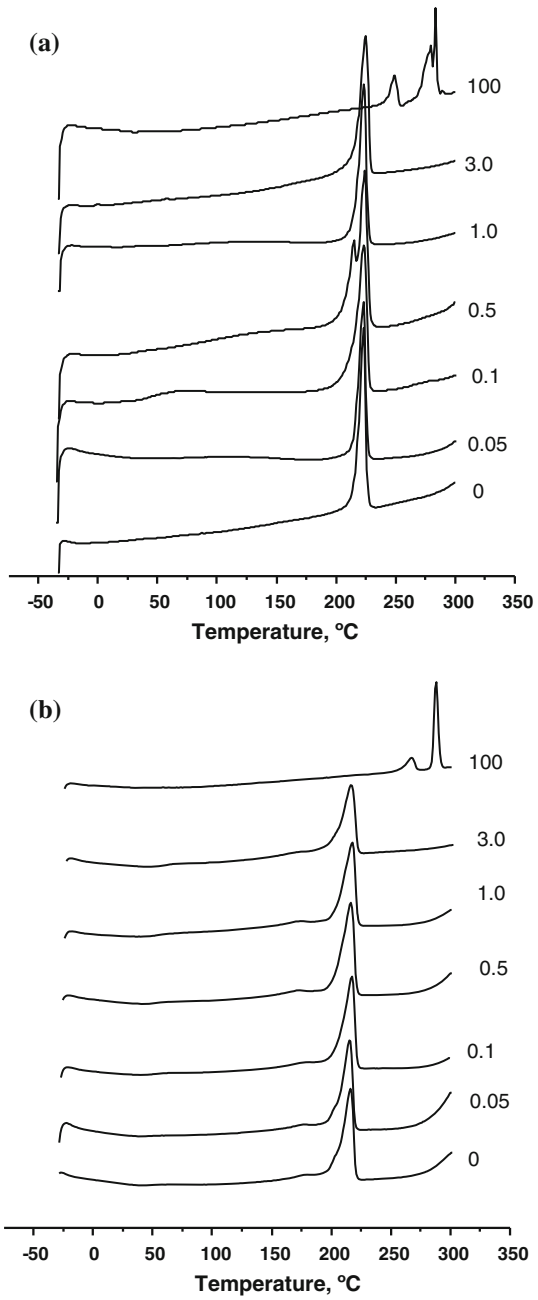

Fig. 6 DSC scans with PA6/PCBM samples with various amounts of fullerene filler in wt%. **a** First scan, **b** second scan

Table 3 Influence of the PCBM content on the melting temperatures and overall crystallinity index X_c

PCBM (wt%)	First heating		Second heating	
	T_m (°C)	X_c (%)	T_m (°C)	X_c (%)
0	223	43.5	216	19.3
0.05	223	45.8	215	19.2
0.1	223	35.5	215	20.5
0.5	215; 225	40.9	215	19.1
1	223	44.5	216	19.4
3	224	38.0	214	17.0

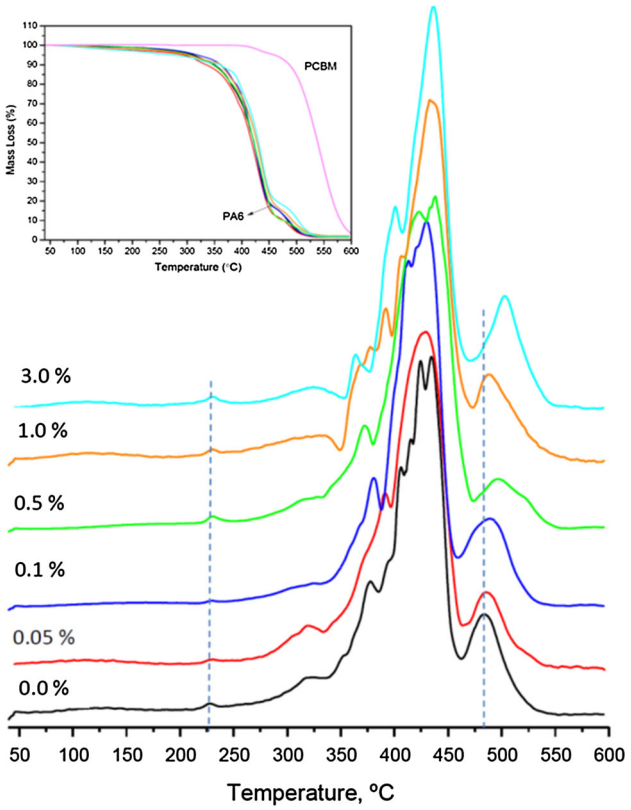

Fig. 7 Derivatized and original (*inset*) TGA curves of PA6/PCBM composites with filler concentrations in the 0–3 wt% range obtained in air atmosphere

prepared composites, most of them display only one melting peak at about 223–225 °C (Fig. 6a) suggesting that the crystalline structure of PA6 matrix is built up essentially by the higher melting α-type crystals. A small shoulder at about 215 °C corresponding to the γ-form was detected by DSC only in the sample containing 0.5 % PCBM. During the second heating, all samples show a single melting peak at 214–216 °C (Fig. 6b; Table 3). This shift of the melting endotherms to low temperatures can be explained with the high cooling rate after the first DSC scan resulting in imperfect crystals of both α-and γ-PA6. For this reason the crystallinity indices X_c determined in the second heating scan are significantly lower than those of the as-prepared composite samples. Interestingly, the two peaks at 275 and 300 °C of PCBM do not appear in the composite with 3 % of this filler in either first or second heating scans. This is one more proof for the involvement of PCBM in unable to melt cross-linked structures.

The PA6/PCBM composites were further studied by TGA. Figure 7 displays the derivatized weight retention

Table 4 Data from the thermo-oxidative degradation of PA6/PCBM composites

PCBM content (wt%)	Temp. of 5 % loss (°C)	Residue at 500 °C (%)	Intervals of degradation and their TMWL (°C)			
			I	II	III	IV
–	306	4.9	320	377	429	483
0.05	310	4.5	325	395	430	486
0.1	321	5.5	327	383	432	491
0.5	307	6.4	332	373	438	500
1.0	300	8	334	393	438	505
3.0	280	11.5	333	404	440	506
100	460	84.5	–	–	–	–

curves and its inset displays the respective integral curves obtained in air atmosphere, i.e., under conditions favoring the thermo-oxidative degradation. The original TGA curves (Fig. 7, inset) and the numerical data extracted from them (Table 4, columns 1–3) show that as a result of thermo-oxidative degradation, the pure PCBM produced 5 % weight loss at 460 °C and the neat PA6 at 306 °C. In the PA6/PCBM composites with 1 and 3 % PCBM, the same loss was registered at 300 and 280 °C, respectively. Such unexpected decrease was not reported for PA6/C_{60} systems. It can be explained with the presence of ester groups in PCBM molecule, whose reaction with the amide group of the PA6 matrix at temperatures close to 300 °C could catalyze its incipient degradation. Increasing the PCBM content from 0.05 to 3 %, the residue at 500 °C grew from 4.5 to 11.5 %. At weight losses close to 80 %, the slopes of all integral curves change, suggesting the presence in all composites of a PA6 fraction being more resistant to degradation.

A more rigorous analysis of the thermo-oxidation behavior is possible on the basis of the derivatized TGA curves. Leaving out of account the process at 250 °C that can be related to degradation of small amounts of oligomeric products, the curves in Fig. 7 can be divided into four characteristic intervals. Table 4, columns I–IV, summarizes the temperatures of the maximum weight losses (TMWL) in each interval. In all of the samples, TMWL increase with the increase of PCBM content. The highest growth is registered in the fourth temperature interval, where the temperatures vary in the 480–510 °C range.

The TGA results of this study are in good agreement with the previously reported stabilizing effect of fullerenes against thermo-oxidative degradation of polymers [27–29]. As the temperature increases, the decomposition of PA6 passes through the formation of hydroperoxide moieties at the methylene group directly bonded to the amide N atom [30]. Subsequently, a number of alkyl- and oxygen-containing radicals are formed propagating the degradation process. According to Troitzkii et al. [31], fullerene and its derivatives can react with such radicals forming more stable compounds thus retarding the thermo-oxidation.

In order to analyze the influence of PCBM on the molecular structure and relaxation processes in PA6, DMTA measurements were performed. Data of storage modulus (E') and loss tangent (tan δ) versus temperature are shown in Fig. 8 for the matrix PA6 (curves 1 and 3) and the composite containing 3 wt% of PCBM (curves 2 and 4). The two E' curves indicate high material stiffness at low temperatures, which decreases considerably just before the appearance of certain relaxation processes. The magnitude

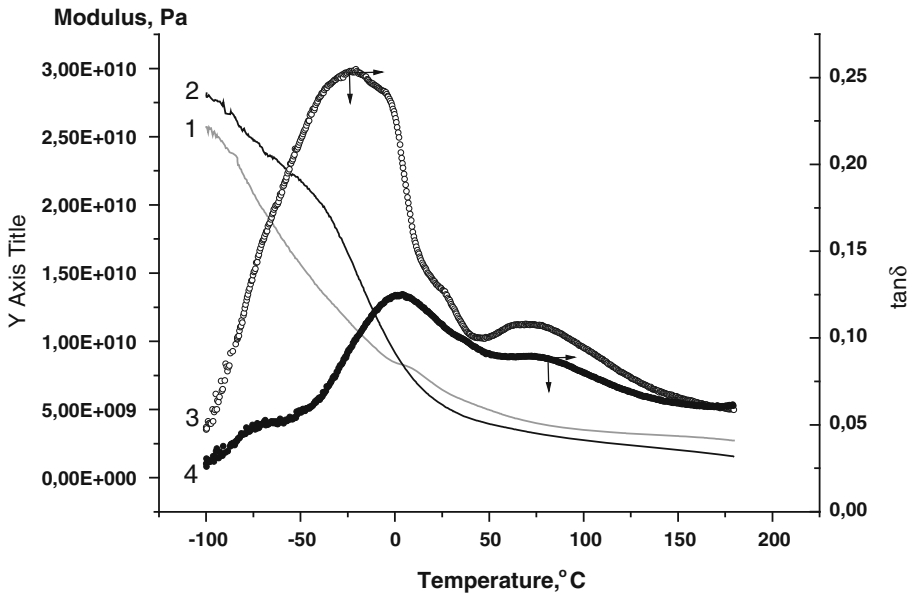

Fig. 8 Temperature dependence of the storage modulus E' and loss tangent tan δ for neat PA6 (1 and 3), PA6 with 3 wt% of PCBM (2 and 4)

of E' is higher for the composite than for the unmodified PA6 only up to 0 °C. Above this temperature, the stiffer material is the neat PA6 matrix. This behavior is different as compared to that of PA6/CNT [32] or PA6/clay composites [33] obtained by melt mixing, in which the composite materials displayed higher E' moduli in the whole temperature range studied.

The neat PA6 and the composite show two loss tan δ peaks in the above temperature range (Fig. 8, curves 3 and 4) labeled as β- and α-transition. The maximum of the higher-temperature α-relaxation is assigned to the glass transition temperature T_g of the PA6, which involves the motion within the amorphous region and depends on the polymer crystallinity. [34] The low-temperature β damping peak is attributed to the motions of the PA6 carbonyl group able to form hydrogen bonds.

Both damping tan δ peaks of the composite are shifted to higher temperatures with ca. 25 °C for β-transition and about 10 °C for the α-transition. This shift is an indication for a more limited motion in the PA6/PCBM system for both C=O groups and whole molecular segments resulting, respectively, in limited capability for H-bond formation and a higher T_g. The peak area under the tan δ curve at the glass transition is quantified by the energy dissipated during the dynamic experiment and gives information about the viscous parts of the composites [35]. The intensity reduction of the tan δ in the area of T_g for the PA6/PCBM composite reflects high volume of constrained PA6 chains in this system, most probably resulting from extensive interaction with the PCBM. This can be considered as an additional and independent indication in favor of the grafting of PA6 on the C_{60} spheroid resulting in the formation of cross-linked network structures.

Morphology by SEM

The surface topography by SEM of neat anionic PA6 and of the PA6/PCBM composite containing 3 wt% of fullerene derivative produced via in situ AAROP of ECL is shown in Fig. 9. As expected, the micrograph of the cryofractured neat anionic PA6 (Fig. 9a) did not show any specific morphology at micro- and nanometer length scale. The sample with relatively high amount of PCBM (Fig. 10b) displayed quite interesting surface topology. It included finely dispersed spherical particles with average diameters in the 20–30 nm range co-existing with bigger, cauliflower-like aggregates with sizes slightly below 1 μm. No voids or visible cracks are observed at the interface between the matrix and the spherical nanoparticles, or between the grains in the bigger aggregates which can be ascribed to a good adhesion at the respective interfaces. Both nano- and microsized morphologies must have been formed at the stage of solid-state AAROP, since PCBM was soluble in ECL monomer at molecular level. A possible explanation of the nanostructure observed in the PA6/PCBM systems is given further in the text.

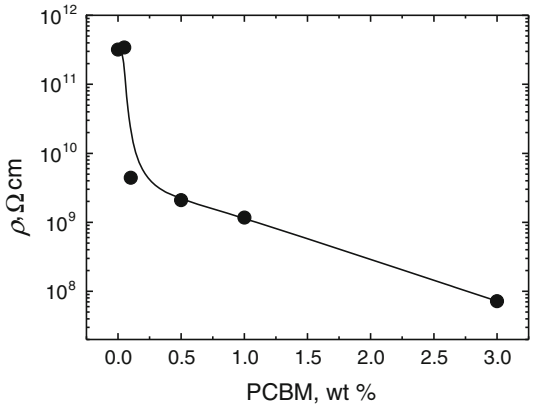

Fig. 10 Volume resistivity ρ [Ω cm] of in situ PA6/PCBM composites as a function of the fullerene compound concentration

Volume resistivity measurements

The neat PA6, as most polymeric materials, is an inherent insulator and can, therefore, accumulate electrical charges

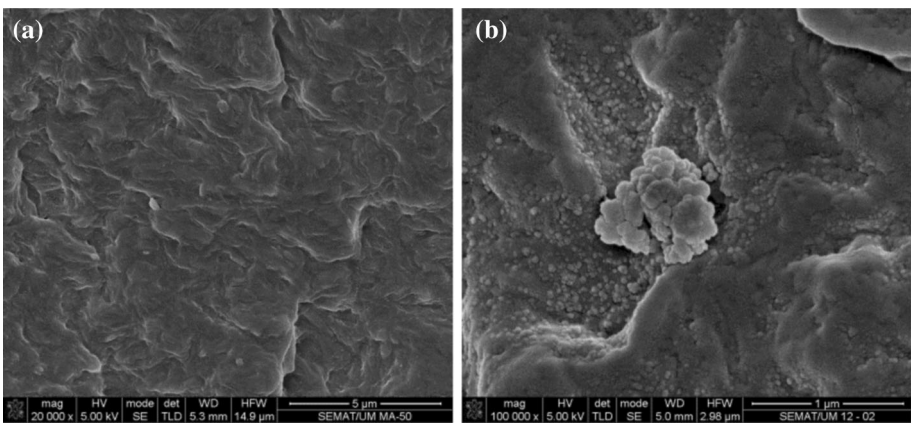

Fig. 9 SEM microphotographs of samples prepared by in situ AAROP of ECL. **a** Neat PA6, **b** PA6-based composite with 3 wt% of PCBM

during its manufacturing, handling, or exploitation. To mitigate electrostatic charges thus avoiding spontaneous static discharge events, antistatic or static dissipative materials are needed with volume resistivities in the range of 10^6–10^{10} Ω cm [36]. A possible way to improve the electrical conductivity of an insulator is the incorporation of uniformly dispersed charge carriers. As indicated earlier [16], C_{60}/C_{70} fulleroid soot fillers could serve as such charge carriers in anionic PA6. In the present study, the electrical volume resistivity ρ at 23 °C of in situ PA6/PCBM composites comprising 0.05–3.0 wt% of conductive filler was measured and presented in Table 5 and Fig. 10.

Figure 10 shows a two-step decrease of the composite resistivity ρ with the increase of the PCBM concentration. First, a steep decline from $\rho = 3.2 \times 10^{11}$ to 3.2×10^9 Ω cm is observed with only 0.1 wt% of the filler, usually denoted as supralinear behavior. It is followed by a constant, linear decline from 2.1×10^9 to 7.2×10^7 Ω cm for PCBM concentrations up to 3 wt%. Similar supralinear behavior was observed in ceramics systems [37]. Small amounts of TiO_2 (less than 8 %) introduced into Ta_2O_5 matrices increased abruptly the dielectric constant of the matrix. Above this concentration, the electrical and optical properties returned to the predicted linear regime. This behavior was related to a 4.5 % decrease of the molecular volume and a nearly 6 % increase of the molecular polarizability. For the PA6/PCBM composites of the present study, it can be assumed that PCBM acts as a joint molecule within the PA6 matrix structure facilitating the electron transport between two conjugated π-bonds of two C_{60} spheroids. Apparently, this effect has a major influence on ρ for low PCBM concentrations. As the percentage of the PCBM increases above 1 wt%, the resistivity of the system starts to be governed by the intrinsic resistivity of PCBM. To the best of our knowledge, there are no consistent data on the bulk resistivity of PCBM. This parameter will strongly depend on the sample preparation conditions and to consider them all a separate study will be necessary. At this point, a conclusion could be made that less than 3 wt% of PCBM can decrease the ρ values of a PA6/PCBM thermoplastic composite obtained by reactive processing by four orders of magnitude, which is sufficient to produce static dissipative materials. It should be noted that the abrupt initial decrease of ρ for PCBM content of 0.1 wt% is not accompanied by structural changes. Above 0.5 wt% of PCBM, however, the gradual decrease of ρ is accompanied by intensive crosslinking of the PA6/PCBM system that could have a strong effect on the mechanical properties. Which one of the concentration ranges will be preferred will depend on the mechanical and electrical properties required.

Mechanism of the in situ AAROP of ECL in the presence of PCBM

The critical analysis of the experimental results allows the supposition that the AAROP of ECL will proceed by different mechanisms depending on the proximity of the fullerene spheroid and its π-electron conjugated system. Let us first consider the interaction between the molten ECL monomer and PCBM at 100 °C. Based on our UV–Vis and X-ray studies before AAROP and having in mind previous works on the interaction of C_{60} fullerenes with primary and secondary amines [24, 25], it seems that the ECL–PCBM interaction passes through mutual orientation of the two molecules, subsequent formation of ion-radicals and zwitter ions, finally resulting in chemical bonding of ECL to fullerene (Scheme 2, I). It should be noted that the attached ECL moiety loses its amidic H-atom which bonds to the adjacent C-atom of a C_{60} benzene ring. The big excess of ECL in respect to PCBM makes probable the attachment of several ECL fragments per fullerene spheroid as shown schematically in structure 2. This will upset the conjugation of the PCBM spheroid causing changes of the UV/Vis absorbance and the X-ray diffraction peaks of the low-molecular compounds 1 and 2 that will depend on the number of bounded ECL moieties.

The addition of DL introduces the ECL anion, the initiator of the polymerization process. This anion will attack the carbonyl group of the lactam ring attached to C_{60} and cause its opening (Schemes 2, 3) producing another change of the UV–Vis absorbance. Structure 3 represents a highly reactive secondary amine anion that will easily abstract a proton either from the NH group of the ECL monomer (with recuperation of the initiating ECL anion) or from the neighboring CH_2 group of C_{60}, thus restoring the initial conjugated π-electron system before the ECL bonding. Which of the two processes will predominate will depend on steric factors. Thus, the stabilized structure 3 already

Table 5 Volume resistivity ρ of PA6/PCBM composites obtained by AAROP as a function of the PCBM concentration

PCBM content (wt%)	0	0.05	0.1	0.5	1.0	3.0
Thickness (cm)	0.35	0.36	0.36	0.36	0.38	0.45
Area (cm^2)	1.33	1.33	1.33	1.33	1.33	1.33
ρ (Ω cm)	3.19×10^{11}	3.42×10^{11}	3.23×10^9	2.1×10^9	1.17×10^9	7.2×10^7

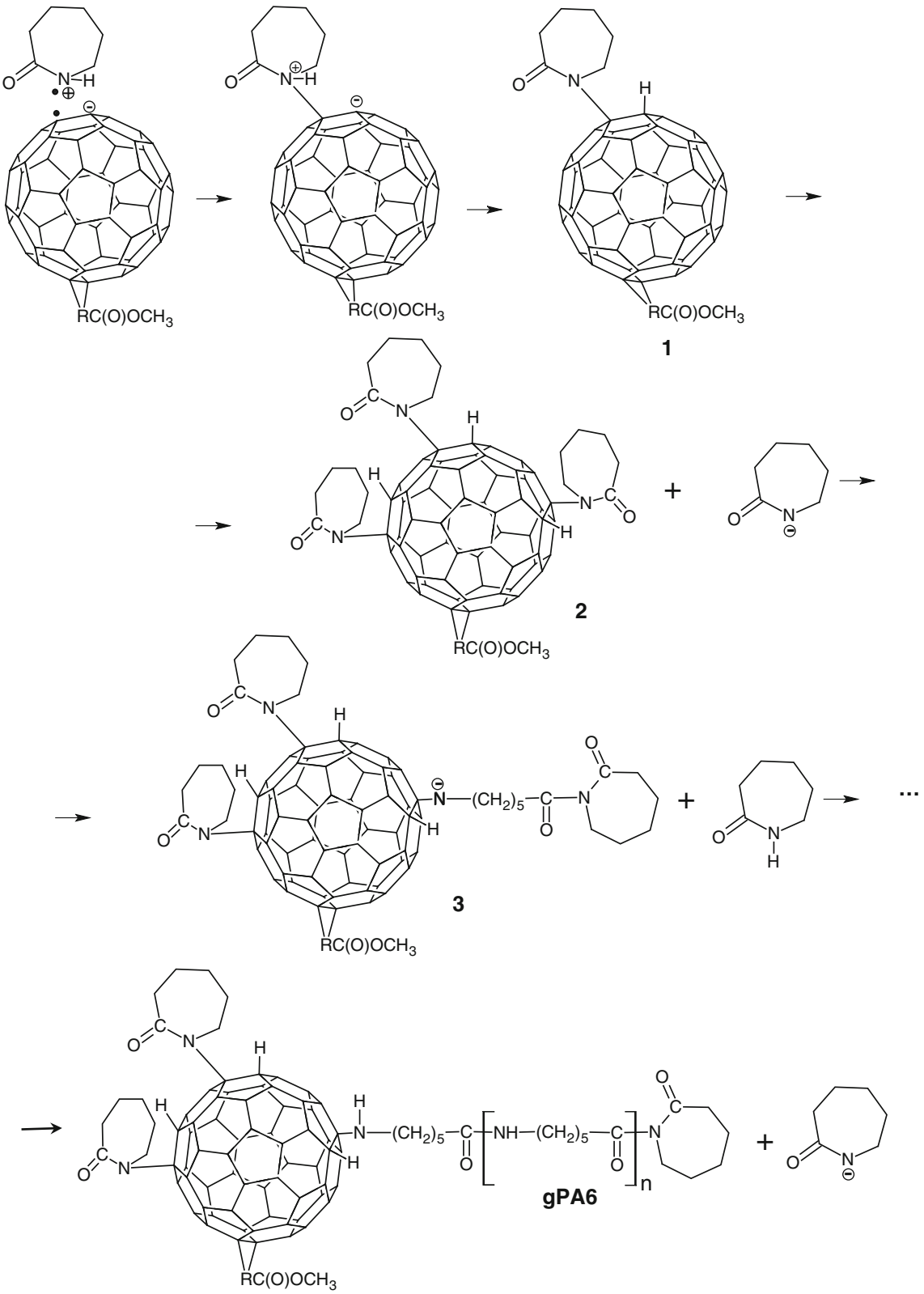

Scheme 2 Suggested mechanism of ECL/PCBM interaction and PA6 grafting on PCBM spheroid

contains the imide link O=C–N–C=O which is activator of AAROP and accelerates the addition of ECL monomer units so that the grafted PA6 (gPA6) linear chain grows from the chain end that is away from the fullerene spheroid. It is believed that the conditions are present for all ECL moieties attached to the same C_{60} spheroid to react in a similar way; hence, several ongoing grafted PA6 chains will be formed producing star-burst PA6–PCBM structures.

Away from the fullerene spheroids, the AAROP of ECL will proceed according to a well-known scheme (Scheme 3). First, the activator C20 (Scheme 1, II) and the initiator DL (Scheme 1, I and III) react to form a carbanion that subsequently abstracts a proton from a monomer molecule to recuperate the initiating ECL anion. The chain propagation proceeds through an attack of the ECL anion on the activating imide linkage found in the beginning of each chain. A new carbanion is produced being with one ECL unit longer and the ECL anion is restored. It should be noted that C20 comprises two imide linkages so the chain propagation to linear PA6 will be realized in two opposite directions simultaneously.

In this study, intensive gel fraction formation reaching 80 % of the polymer weight was registered when AAROP was carried out in the presence of 0.5–3 wt% of PCBM. To the best of our knowledge, such phenomenon is reported for the first time in PA6/fullerene systems. Interestingly, no gel fraction was produced in neat PA6 and in the composites with 0.05 and 0.1 wt% of PCBM obtained at the same AAROP conditions. This means that the chemical crosslinking which is the typical reason for gel formation is somehow related with the fullerene structure.

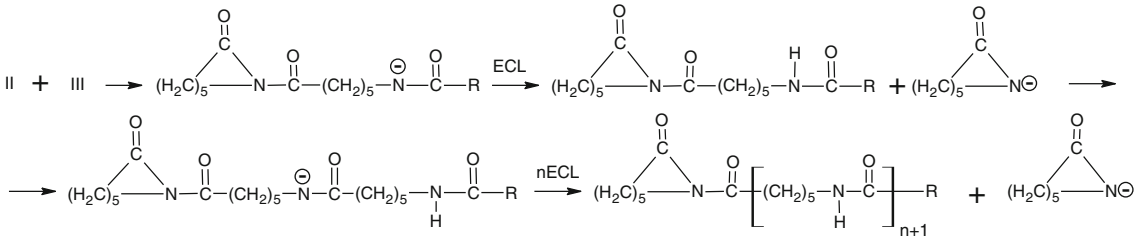

Scheme 3 AAROP of ECL away from fullerene spheroid according to Ref. [38]

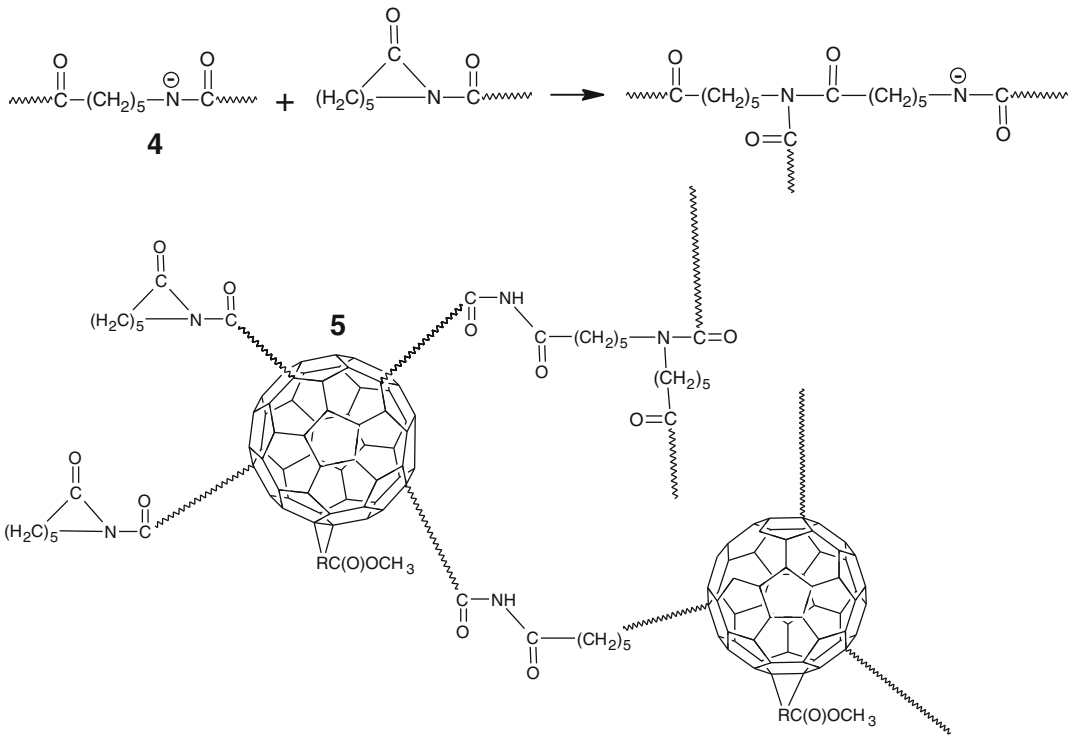

Scheme 4 Supposed formation mechanism and structure of the PA6–PCBM gel fraction

Theoretically, AAROP of ECL can result in gel fraction formation when the polymeric carbanion (Scheme 4, structure 4), instead of abstracting a proton from ECL, reacts with the imide linkage positioned in the beginning of another PA6 chain. This creates a point of crosslinking and provides another carbanion that can react similarly. The mechanism of crosslinking in Scheme 4 will predominate if two conditions are present: (1) low concentrations of ECL monomer which is the main source of protons to compensate the carbanions in the propagation step of normal AAROP (Scheme 3), and (2) elevated concentration of imide links found in the beginning of each PA6 macromolecule. As seen from Scheme 2, structures 3 and 4, in the presence of PCBM, several ECL molecules can attach to the C_{60} spheroid losing their amidic protons. Structure 5 in Scheme 4 also shows that each of the many linear PA6 branches originating from a C_{60} spheroid end with an imide linkage. This means that the exhaustion of ECL (i.e., by the end of AAROP) and increasing the PCBM concentration will satisfy both conditions and result in more pronounced gel fraction formation, which is exactly what was registered in the viscosimetric measurements of this study. Structure 5 allows the conclusion that the gel fraction should include most of PCBM molecules, whereby each of them will be chemically interlaced in a network thus losing the capacity to crystallize separately. The DRIFTS, DSC, and DMTA measurements are in agreement with such supposition. The spherical morphologies found in the PA6/PCBM composites in the nanometer length scale and their aggregates can also be related to a profound chemical interaction between the substituted fullerene spheroids and the linear PA6 chains according to Scheme 4.

Summary

In situ preparation of PA6/PCBM composites by activated anionic polymerization of ECL passes through a complex interaction between the monomer and the π-electron system of the fullerene spheroid. Based on structure investigations at various stages of the process by UV/Vis, WAXS, DRIFTS, DSC, TGA, DMTA, SEM, and viscosimetric measurements, a mechanism of the polymerization process was suggested that agrees with all experimental data obtained. According to it, in the composites comprising 0.5–3.0 wt% PCBM strong crosslinking between the linear PA6 chains and the substituted C_{60} moieties takes place resulting in a unique sample morphology that comprises nanosized spheres co-existing with micron-sized cauliflower-shaped aggregates built by both PCBM and PA6. Volume resistivity measurements indicate that PCBM concentrations above 0.1 wt% could decrease ρ from 10^{11} Ω cm to 10^{9}–10^{7} Ω cm. Controlling the PCBM percentage and the AAROP conditions has the potential to tailor the composite structure and properties and thus to improve the electrical and thermal conductivity for technological applications in mitigation of spontaneous static discharge events.

Acknowledgements This work was supported by FCT (Fundação para a Ciência e Tecnologia—Portugal) through the program Strategic Project LA 25 2013–2014 and by the European Regional Development Fund (FEDER) through COMPETE, project EXPL/CTM-POL/0933/2012. N. Dencheva is grateful to the FCT for supporting her research by the postdoctoral award SFRH/BPD/45252/2008, co-financed by QREN–POPH program of the European Union. The financial support of HASYLAB at DESY (Grant No. II-07-011 EC) is also gratefully acknowledged. The authors wish to thank Mauricio Malheiro for his technical assistance in the DMTA and UV-Vis experiments.

References

1. Vanlaeke P, Swinnen A, Haeldermans I, Vanhoyland G, Aernouts T, Cheyns T, Deibel C et al (2006) P3HT/PCBM bulk heterojunction solar cells: relation between morphology and electro-optical characteristics. Sol Energy Mater Sol Cells 90:2150–2158
2. Xu H, Li J, Leung BHK, Poon CCY, Ong BS, Zhang Y, Zhao N (2013) A high-sensitivity near-infrared phototransistor based on an organic bulk heterojunction. Nanoscale 5:11850–11855
3. Benjamin SC, Arzhang A, Briggs AD, Britz DA, Gunlycke D, Jefferson J et al (2006) Towards a fullerene-based quantum computer. J Phys Condens Matter 18:S867–S883
4. Wang C, Guo ZX, Fu S, Wu W, Zhu D (2004) Polymers containing fullerene or carbon nanotube structures. Prog Polym Sci 29:1079–1141
5. Jin X, Hu JY, Tint ML, Ong SL, Biryulin Y, Polotskaya G (2007) Estrogenic compounds removal by fullerene-containing membranes. Desalination 214:83–90
6. Dyakonov V, Zoriniants G, Scharber M, Brabec JC, Janssen RAJ, Hummelen JC, Sariciftci NS (1999) Photoinduced charge carriers in conjugated polymer–fullerene composites studied with light-induced electron-spin resonance. Phys Rev B 59:8019–8025
7. Brabec CJ, Johansson H, Cravino A, Sariciftci NS, Comoretto D, Dellepiane G, Moggio I (1999) The spin signature of charged photoexcitations in carbazolyl substituted polydiacetylene. J Chem Phys 111:10354–10361
8. Lu Z, He C, Chung TC (2001) Composites of multifunctional benzylaminofullerene with low density polyethylene. Polymer 42:5233–5237
9. Baltá-Calleja FJ, Giri L, Asano T, Mieno T, Sakurai A, Ohnuma M, Sawatari C (1996) Structure and mechanical properties of polyethylene–fullerene composites. J Mater Sci 31(19):5153–5157. doi:10.1007/BF00355918
10. Weng D, Lee HK, Levon K, Mao J, Scrivens WA, Stephens EB, Tour JM (1999) The influence of Buckminster fullerenes and their derivatives on polymer properties. Eur Polym J 35:867–878
11. Brabec CJ, Dyakonov V, Sariciftci NS, Graupner W, Leising G, Hummelen JC (1998) Investigation of photoexcitations of conjugated polymer/fullerene composites embedded in conventional polymers. J Chem Phys 109:1185–1195
12. Campbell K, Gurun B, Sumpter BG, Thio YS, Bucknall DG (2011) Role of conformation in π–π interactions and polymer/fullerene miscibility. Phys Chem B 115:8989–8995

13. Bucknall DG, Bernardo G, Shofner ML, Nabankur D, Raghavan D, Sumpter BG, Sides S et al (2012) Phase-morphology and molecular structure correlations in model fullerene–polymer nanocomposites. Mater Sci Forum 714:63–66
14. Dencheva N, Denchev Z (2013) Clay distribution and crystalline structure evolution in polyamide 6/montmorillonite composites prepared by activated anionic polymerization. J Appl Polym Sci 130:1228–1238
15. Kelar K (2006) Polyamide 6 modified with fullerenes prepared via anionic polymerization of ε-caprolactam. Polimery 51:415–424 (in Polish)
16. Zuev VV, Ivanova IG (2012) Mechanical and electrical properties of polyamide-6-based nanocomposites reinforced by fulleroid fillers. Polym Eng Sci 52:1206–1211
17. Zuev VV, Shlikov AV (2012) Polyamide 12/fullerene C_{60} composites: investigation on their mechanical and dielectric properties. J Polym Res 19:9925–9930
18. Zuev VV, Kostromin SV, Shlikov AV (2012) Mechanics of polymer nanocomposites modified with fulleroid nanofillers. Vysokomol Soedin Ser A 52:815–819
19. Ivanova L, Kulichikhin SG, Alkaeva OF, Akimushkina NM, Vyrsky UP, Malkin AY (1978) Determining of molecular characteristics of polycaproamide. Vysokomol Soedin Ser A 20(12): 2813–2816
20. POLAR, version 2.7.3; Copyright® 1997–2008 by Stonybrook Technology and Applied research, Inc, USA
21. Roda J (2009) Polyamides. In: Dubois P, Coulembier O, Raquez J-M (eds) Handbook of ring-opening polymerization. Wiley-VCH, Weinheim, p 177
22. Dan F, Vasiliu-Oprea C (1998) Anionic polymerization of caprolactam in organic media: morphological aspects. Colloid Polym Sci 276:483–495
23. Wudl F, Hirsch A, Khemani KC, Suzuki T, Allemand PM, Kosch A et al (1992) Survey of chemical reactivity of C_{60}, electrophile and dieno-polarophile par excellence. ACS Symp Ser 481: 161–175
24. Hirsch A, Brettreich M (2005) Fullerenes: chemistry and reactions. Wiley-VCH, Weinheim, p 87
25. Prato M (1999) Fullerene materials. In: Hirsch A (ed) Topics in current chemistry. Fullerenes and related structures, vol 199. Springer, Berlin, pp 173–187
26. Dencheva N, Nunes T, Oliveira JM, Denchev Z (2005) Microfibrillar composites based on polyamide/polyethylene blends. 1. Structure investigations in oriented and isotropic polyamide 6. Polymer 46:887–901
27. Krusic PJ, Wasserman E, Parkinson BA, Malone B, Holler ER Jr, Keizer PN et al (1991) Electron spin resonance study of the radical reactivity of C_{60}. J Am Chem Soc 113:6274–6275
28. Morton JR, Preston KF, Krusic PJ, Hill SA, Wasserman E (1992) The dimerization of fullerene RC_{60} radicals [R = alkyl]. J Am Chem Soc 114:5454–5455
29. Troitskii BB, Troitskaya LS, Anikina LI, Denisova VN, Novikova MA, Khokhlova LV (2001) Inhibiting effect of fullerenes C_{60} and C_{70} on high-temperature oxidative degradation of copolymers of methyl methacrylate with methacrylic acid and methacrylamide. J Polym Mater 48:251–265
30. Pearce EM, Shalaby SW, Barker RH (1975) Retardation of combustion of polyamides. In: Lewin M, Atlas SM, Pearce EM (eds) Flame retardant polymeric materials. Plenum, New York, pp 239–275
31. Troitskii BB, Troitskaya LS, Dmitriev AA, Yakhnov AS (2000) Inhibition of thermo-oxidative degradation of poly(methyl methacrylate) and polystyrene by C_{60}. Eur Polym J 36: 1073–1084
32. Kelar K, Jurkowski B (2007) Properties of anionically polymerized ε-caprolactam in the presence of carbon nanotubes. J Appl Polym Sci 104:3010–3017
33. Wilkinson AN, Man Z, Stanford JL, Matikainen P, Clemens ML, Lees GC et al (2006) Structure and dynamic mechanical properties of melt intercalated polyamide 6/montmorillonite nanocomposites. Macromol Mater Eng 291:917–928
34. Jha A, Bhowmick AK (1998) Thermal degradation and ageing behavior of novel thermoplastic elastomeric nylon-6/acrylate rubber reactive blends. Polym Degrad Stab 62:575–586
35. Shen L, Du Q, Wang H, Zhong W, Yang Y (2004) In situ polymerization and characterization of polyamide-6/silica nanocomposites derived from water glass. Polym Int 53:1153–1160
36. ANSI/ESD S541-2008: packaging material standards for ESD sensitive items (2008)
37. Busani T, Devine RAB (2005) The importance of network structure in high-*k* dielectrics: $LaAlO_3$, Pr_2O_3, and Ta_2O_5. J Appl Phys 98:44102
38. Odian G (2004) Principles of polymerization, 4th edn. Wiley, Hoboken, pp 575–577